CrystEngComm

Accepted Manuscript

This is an *Accepted Manuscript*, which has been through the Royal Society of Chemistry peer review process and has been accepted for publication.

Accepted Manuscripts are published online shortly after acceptance, before technical editing, formatting and proof reading. Using this free service, authors can make their results available to the community, in citable form, before we publish the edited article. We will replace this *Accepted Manuscript* with the edited and formatted *Advance Article* as soon as it is available.

You can find more information about *Accepted Manuscripts* in the Information for Authors.

Please note that technical editing may introduce minor changes to the text and/or graphics, which may alter content. The journal's standard Terms & Conditions and the Ethical guidelines still apply. In no event shall the Royal Society of Chemistry be held responsible for any errors or omissions in this *Accepted Manuscript* or any consequences arising from the use of any information it contains.

ROYAL SOCIETY OF CHEMISTRY

www.rsc.org/crystengcomm

Please do not adjust margins

Journal Name

ARTICLE

Synthesis, Magnetic and Optical Properties of Nanocrystalline Alkaline-Earth Hexaborides

Lihong Bao[a, †], Xiaoping Qi[a], Tana[a], Luomeng Chao[b], O. Tegus[a]

Cubic-shaped ultrafine alkaline-earth hexaborides (MB_6, M=Ca, Ba, Sr) have been synthesized via a solid-state reaction of MO with $NaBH_4$ at 1150 °C. Phase composition, grain morphology, microstructure, magnetic and optical absorption properties were investigated by using XRD, FESEM, HRTEM, SQUID magnetometer and optical measurements. Results show that all the synthesized hexaborides are composed of CsCl-type single phase and the average grain sizes of CaB_6, SrB_6 and BaB_6 nanocrystalline are 150 nm, 20 nm and 30 nm at the reaction temperature of 1150 °C. The magnetic measurement results show that all the synthesized samples have a weak ferromagnetic behavior at room temperature. This is our first time to found the ferromagnetic property from nanocrystalline alkaline-earth hexaborides. Moreover, the HRTEM results strongly supported that the magnetic moment of alkaline-earth hexaborides is originated from the intrinsic defects of nanocrystals. The optical absorption results show the strong light absorption in visible light region and transparency in near infrared rays for nanocrystalline alkaline-earth hexaborides. This interesting optical property should have important effects for extending the optical applications such as near infrared filtering or detectors.

1. Introduction

The divalent alkaline-earth hexaborides MB_6 (M=Ca, Ba, Sr) crystallized into the CsCl-type cubic structure with a space group of *Pm-3m* symmetry, where metal atoms locate in (0, 0, 0) site and octahedral boron atoms locate in (0.5, 0.5, x) site. As an internal parameter, the x determines the ratio between inter-octahedron and intra-octahedron B-B distances [1-6]. Due to the strong covalent bond of B-B atoms in this structure, it gives rise to the excellent properties of the high melting point, the high chemical stability and the high hardness, as well as other novel properties of the low work function and the low coefficient of thermal expansion. Thanks to their excellent advantages, the alkaline-earth hexaborides are potential applied for electron sources[7-9] and thermoelectric materials[10-12]. Since 1999, the high temperature ferromagnetism of La-doped CaB_6 single crystal was discovered by Young et al [13], it has attracted many attentions to interpret its origin of the special magnetism by both experimentally and theoretically because there absence of 3*d* or 4*f* electrons associated with magnetic order [14]. Subsequently, Lofland *et al* [15], Dorneles *et al* [16], Ackland *et al* [17] and Zhao *et al* [18] also found the weak ferromagnetism from undoped CaB_6, SrB_6, BaB_6 single crystal or thin films at an ambient temperature and their magnetism are believed to induce by the intrinsic defects. In addition, there are also some other explanations for the origin of magnetism such as ferromagnetic impurities phases

[a] *Inner Mongolia Key Laboratory for Physics and Chemistry of Functional Materials, Inner Mongolia Normal University, Hohhot 010022, China*
[b] *Shenyang National Laboratory for Materials Science, Institute of Metal Research, Chinese Academy of Sciences, 72 Wenhua Road, Shenyang 110016, China*
† *Email:baolihong@imnu.edu.cn. Tel.: (+86) 471-4393242.*

CrystEngComm Accepted Manuscript

attributing to ferromagnetism [19-21]. Therefore, the magnetic properties of alkaline-earth hexaborides are still a research hot topic to need further studying. However, up to now the magnetic properties of nanorystalline alkaline-earth hexaborides have been very rarely reported.

It is well known that rare-earth hexaborides (RB_6) have a similar CsCl-type structure to alkaline-earth hexaborides and exhibits many excellent mechanical and electron emission properties [22-25]. More recently, the nanoparticle of rare-earth hexaborides demonstrated a strong light absorption in near infrared rays (NIR) and transparency in visible light (VL), which is resulted from the free electron plasmon resonance [26-28]. This interesting optical characteristic is well satisfied the demand for reducing solar heat for the windows of automotive and architecture, and also have potential applications in medical care. However, the optical properties of nanocrystalline alkaline-earth hexaborides have been very rarely reported so far in the literatures. Whether the alkaline-earth hexaborides also possess a various interesting optical absorption properties is our another research purposes in present work.

In this paper, we have successfully fabricated the ultrafine alkaline-earth hexaborides and investigated their magnetic and optical absorption properties for the first time. As a result, the grain size and morphology of synthesized samples are very sensitive to the reaction temperature. The magnetic measurement results indicated all the synthesized samples show a weak ferromagnetic behaviour at room temperature. The optical absorption results show the nanocrystalline alkaline-earth hexaborides exhibited a strong light absorption in visible light and transparency in near infrared rays, which is much different from the rare-earth hexaborides. This interesting optical property should have important effect on extending the optical applications such as near infrared filtering or detectors.

2. Experimental

Raw materials: Calcium oxides (99.9% purity, Sigma-Aldrich), Strontium oxides (99.9% purity, Sigma-Aldrich), Barium oxides (99.95% purity, Aladdin) and Sodium borohydride (99.0 purity, Sigma-Aldrich) powder in a fixed molar ratios were mixed in an agate mortar for an hour. The mixtures were pressed into a plate under the pressure of 5 ton. And then the mixtures were placed into the resistance furnace at a reaction temperature in the range from 900 to 1150 ^{o}C for 2 hours with heating rate 3 ^{o}C/min. Whole reaction was kept under a vacuum of 2×10^{-2} bar. After reaction the products were washed several times by hydrochloric acid, distilled water and anhydrous alcohol.

Characterizations: The phase identification was examined by X-ray diffraction (Cu K_α radiation, Philips PW1830). The scans 2θ were taken between 20 to 80°at 0.05° intervals with a 2s count time. The crystal morphology was characterized by field emission scanning electron microscope (FESEM: Hitachi SU-8010) and the microstructure is characterized by transmission electron microscopy (TEM: FEI-Tecnai F20 S-Twin 200 KV). TGA (Perkin-Elmer TGA 7 system; Ar flow, heating rate: 10 ^{o}C /min). X-ray photoelecreon spectra (XPS) were performed by an Amicus X-ray photoelectron spectrometer using Al X-rays as the excitation source. The magnetic properties were measured by using SQUID magnetometer (Quantum Design MPMS, 7 Telsa). The ultraviolet–visible–near infrared spectrometer (PerkinElmer Lambda 750S) with a tungsten–halogen visible lamp and a deuterium ultraviolet lamp was used to measure the absorption performance.

3. Results and discussion

3.1 Reaction mechanism and phase composition

The thermal analysis as an effective method can analyse the formation and decomposition of the complex combination in the whole procedure, as well as determining the reaction conditions or obtaining the reaction temperature effectively. So it is necessary to study the reaction mechanism. Herein, the synthesis of BaB_6 as an example is analyzed by the Differential Thermal Analysis (DTA) with the heating temperature in the range of 30~1000^{o}C to estimate the decomposing and the formation temperature of reaction products. It can be seen from the Fig.1 that there is a small exothermic reaction peak located at around 390 ^{o}C, which is initially estimated to the melting of barium hydroxide ($Ba(OH)_2$). Because the raw material of

CrystEngComm Accepted Manuscript

 This journal is © The Royal Society of Chemistry 20xx

barium oxide is easy to absorb water from air to form the pure barium hydroxide with the melting point of 400 °C. This temperature is well consistent with the exothermic peak of 390 °C. As for other two strong exothermic peaks of 460 °C and 506 °C, it is maybe caused by the decomposing of $NaBH_4$. At the former temperature of 460 °C, the $NaBH_4$ decomposed into NaH and BH_3. And then, the BH_3 is unstable and easily decomposed into B and H_2, which are well agreement with our previous synthesis of LaB_6 [29] and the results of Ma *et al* [30]. The exothermic peak at 793 °C, it is induced by the NaH decomposing into sodium and hydrogen gas due to its decomposition temperature at 800 °C. Meanwhile, we have found the metal Na has been deposited in cool side of quartz tube after reaction. Based on the above analysis, it can be inferred that the reaction temperature of BaO with $NaBH_4$ to form BaB_6 is higher than 900 °C and the proposed reaction mechanism is summarized as follows:

at 460 °C,

$$NaBH_4(S) \rightarrow NaH(S) + BH_3(S);$$

at 506 °C,

$$BH_3 \rightarrow B(S) + H_2\ (g)$$

at 793 °C,

$$NaH\ (S) \rightarrow Na(S) + H_2\ (g)$$

at higher 900 °C,

$$BaO(S) + B(S) + H_2(g) \rightarrow BaB_6(S) + H_2O\ (g)$$

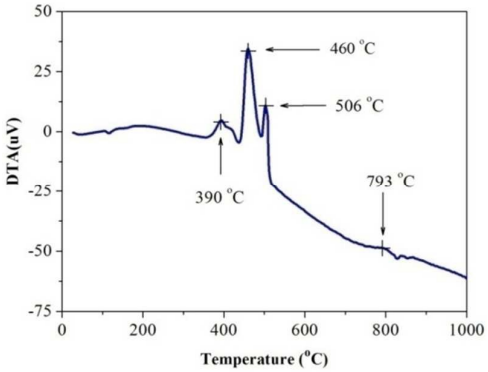

Fig.1 DTA curve for mixture powder of BaO and $NaBH_4$ with a molar ratios of 1:6

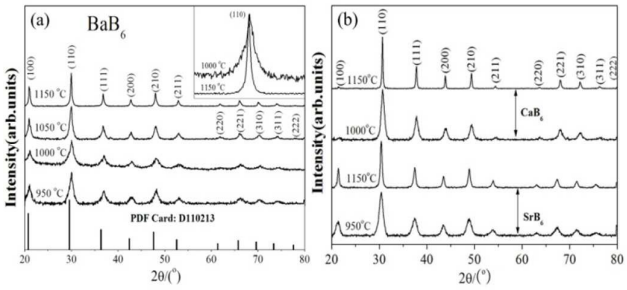

Fig.2 XRD patterns of MB_6 prepared at different reaction temperatures. (a)BaB_6, (b) CaB_6 and SrB_6

In order to accurately determine the synthesis sequence of phase formation, four samples were prepared at different reaction temperatures. It can be seen from Fig.2 (a) that when the initial reaction temperature at 950 °C, the sample is composed of BaB_6 single phase with the space group of *Pm-3m* (PDF Card: D110213) and without any extra impurity peaks of BaO and $NaBH_4$ in the patterns, confirming the high purity of the synthesized products. In addition, this formation temperature is consistent with the estimation results of the TDA measurements. For further increasing the reaction temperatures to 1000 °C, 1050 °C and 1150 °C, all the synthesized samples are composed of BaB_6 single-phase and the diffraction peaks are well indexed and assigned to the parallel crystal plane of (100), (110), (111), (210) and (211). Seeing from the diffraction peaks of insert Fig.2(a), the peak intensity of BaB_6 prepared at 1150 °C is much stronger and its half-peak width is more narrower than that of BaB_6 prepared at 1000°C, indicative of better crystallization and the grain growth behaviours with increasing the reaction temperature. Fig.2 (b) displays the XRD patterns of CaB_6 and SrB_6 nanocrystalline prepared at different reaction temperatures. It shows that all the synthesized samples are identified as CsCl-type single phase without any extra impurity phases. Meanwhile, it is found the diffraction peaks were sharp and well-defined at an elevated temperature, which is also the result of high crystallinity and grain growth.

3.2 The micrograph and microstructure of MB_6 nanocrystalline

CrystEngComm Accepted Manuscript

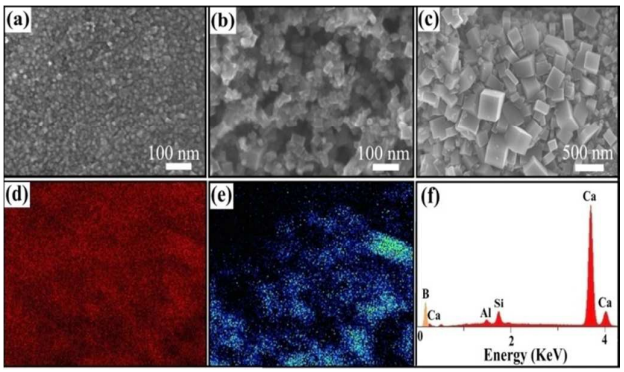

Fig.3 FESEM images of CaB_6 prepared at different reaction temperatures. (a) 1000 ^oC, (b) 1100 ^oC, (c) 1150 ^oC, (d) element mapping for Ca (e) element mapping for B (f) corresponding element spectrum

To further investigate the grain size, surface morphology and element distribution of CaB_6 nanocrystalline prepared at different reaction temperatures, the field emission scanning electron microscopy (FESEM) was used to observe the grain surface morphology. Fig.3 shows the typical FESEM images of CaB_6 nanocrystalline prepared at different reaction temperatures. When the reaction temperature at 1000 ^oC (see Fig.3a), the CaB_6 are mainly composed of ultrafine nanoparticles with a mean size of smaller than 10 nm and without any cubic shape crystals, indicating the reaction products mainly composed by agglomerated nanoparticle at this step. When the reaction temperature increasing to 1100 ^oC, it is obviously found that a large amount of nanoparticle have converted into small crystalline nanocube with a size of 20 nm as shown in Fig.3 (b). For further increasing temperature to 1150 ^oC, the perfect nanocube formed and an obvious grain growth causing the grain size to 150 nm. One of the important factors for the grains growth behaviors is that the high specific surface and high diffusion coefficients of nanoparticle, acting as the nucleation center for the formation of hexaboride cubes, have cause to mass transport through lattice and grain boundaries to grain growth. Fig.3 (d) and Fig.3 (e) shows the element mapping results of Ca and B corresponding to image of Fig.3(c), where the Ca and B elements are distributed homogeneously. The element spectrum of Fig.3 (f) also confirmed that there existed the high content of Ca and B element in selected area. As to emergence of Si elements, it can be interrupted as coming from infiltration of quartz tube through sample surface at higher reaction temperature. The Al elements are mainly from conductive adhesive. But we cannot find any ferromagnetism impurity elements such as iron.

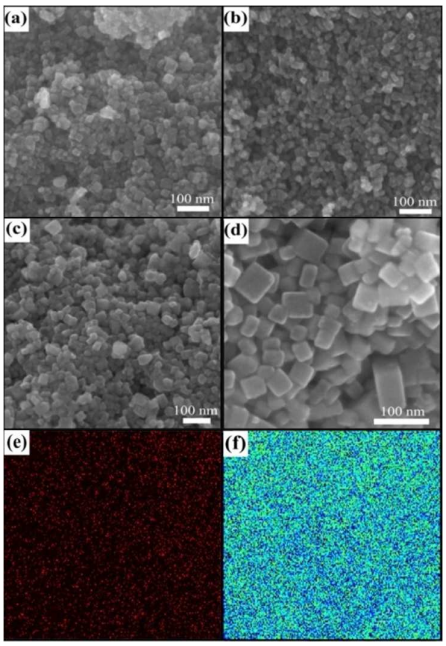

Fig. 4 FESEM images of SrB_6 prepared at (a) 1050 ^oC, (b) 1150 ^oC and BaB_6 prepared at (c) 1050 ^oC, (d) 1150 ^oC, (e) element mapping for B (f) element mapping for Ba

The surface morphology of the SrB_6 and BaB_6 nanocrystalline prepared at 1050 and 1150 ^oC are given in Fig.4. It shows that both the SrB_6 and BaB_6 already crystallized into large amount of ellipsoidal shape crystals and small amount of cubic shape crystals at the reaction temperature of 1050 ^oC as shown in Fig.4 (a) and Fig.4(c). Increasing the reaction temperature to 1150 ^oC, the number of ellipsoidal shape crystals decreased obviously and all of them have transformed into small cubic grains with a grain size of 20 nm and 30 nm as shown in Fig.4 (b) and Fig.4 (d), respectively. This indicates that the higher reaction temperature is beneficial for forming better dispersed nanocrystals with a better cubic shape. Fig.4 (e) and Fig.4 (f) shows the element mapping results of Ba and B corresponding to image of Fig.4(d). It is obviously seen the Ba and B elements are distributed homogeneously indicating a high content of Ba and B element in selected area. However, due to the limitation of FESEM resolution, it is hardly to observe the surface grain

CrystEngComm Accepted Manuscript

This journal is © The Royal Society of Chemistry 20xx

morphology and microstructure of ultrafine SrB_6 nanocrystalline clearly. Thus, in order to obtain the microstructure and EDS information of ultrafine SrB_6 nanocrystalline, the high resolution transmission electron microscope working at 200 kV have completed above mentioned tasks.

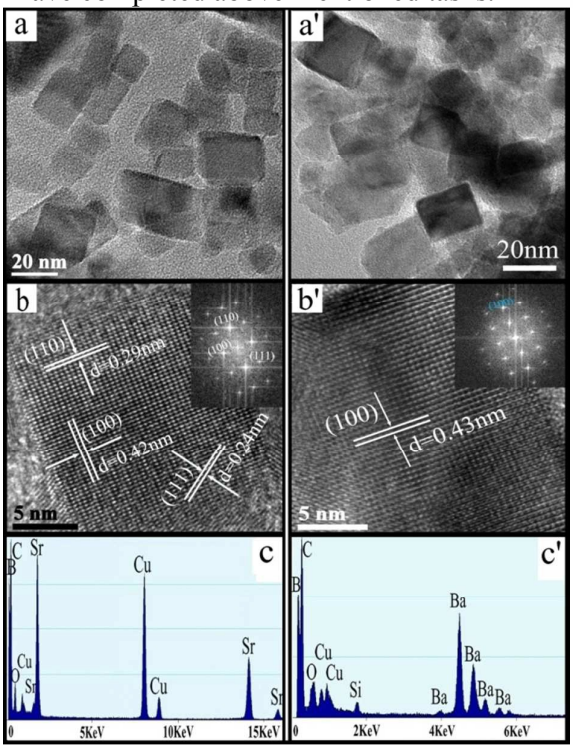

Fig.5 (a) TEM analysis of ultrafine SrB_6 nanocrystalline prepared at 1150 °C, (a′) for BaB_6 (b) the HRTEM image and indexing FFT patterns of SrB_6, (b′) for BaB_6, (c) element spectrum of selected single crystals of SrB_6, (c′) for BaB_6

Fig.5 (a) shows the typical TEM image of ultrafine SrB_6 nanocrystalline. It can be observed that the synthesized hexaborides have a perfect cubic morphology with a mean size of 20 nm, which is agreement with the observation of FESEM results. The single-crystalline nature of SrB_6 crystal is demonstrated by the HRTEM presented in Fig. 5(b). The lattice fringes d=0.42 nm, d=0.29 nm and d=0.24 nm observed in this HRTEM image agree well with the (100), (110) and (111) crystal planes, respectively. Fig.5 (c) shows the EDS analysis of selected single crystal of SrB_6, where presence of Sr and B elements confirmed the high purity of reaction products without any ferromagnetism elements detected. Fig.5 (a′) shows the TEM images of BaB_6 prepared at 1150 ℃. It can be seen that the synthesized BaB_6 nanocrystalline have a cubic morphology with a grain size of 30 nm. As observed from the HRTEM of Fig.5 (b′), each BaB_6 crystal is single crystal, where the clear paralleled fringes are the indexed (100) crystal planes with an interplanar distance of d=0.43 nm. Fig.5 (c′) shows the EDS analysis of selected single crystal, where Ba and B are present as the primary elements without any impurity ferromagnetism element detected. Based on the above characterizations, it can be inferred that the grain size and morphology of CaB_6, SrB_6 and BaB_6 prepared in present work is much different from pervious investigations. We think that the important factor for the formation of the nanocrystalline alkaline-earth hexaborides is attributed to the boron sources. Because when the boron generated from $NaBH_4$ during the decomposition procedure, it should have the homogeneous ultrafine particle size and high activity than that of the direct reacting with micron size boron. In addition, the $NaBH_4$ decomposed into the H_2 gas, which is favour of reducing reaction.

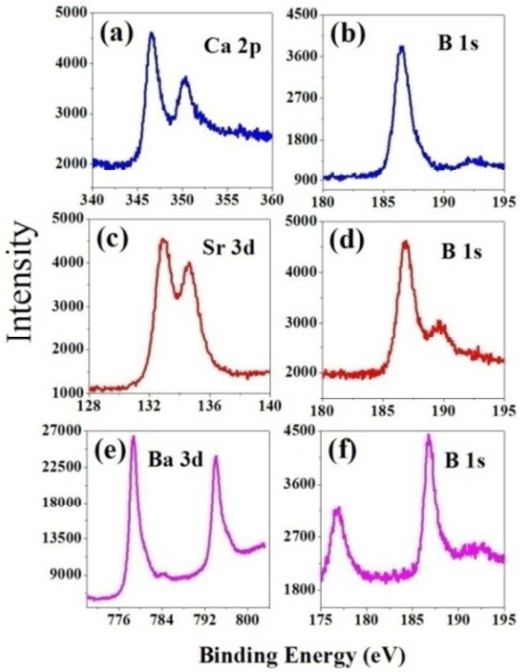

Fig. 6 XPS spectra of CaB_6, SrB_6 and BaB_6

X-ray photoelectron spectroscopy is a powerful technique for identifying the surface species and valence state of synthesized samples. Alkaline-earth hexaborides is belongs to the two valence state compounds and its electronic structure is

CrystEngComm Accepted Manuscript

much different from rare-earth hexaborides. Fig. 6 (a) displays the surface XPS spectroscopy analysis for CaB_6 nanocrystal. The representative spectra of B 1*s* and Ca 3*p* core-level are examined. The binding energy of B 1*s* is equal to 187 eV and that of Ca 3*p* at 346 and 350 eV, which is due to the two atomic orbitals with spin down and spin up in *d* shell. These values well correspond with the works of the S. Angappan *et al* [31]. Fig. 6 (c) and Fig. 6 (e) show the representative spectra for SrB_6 and BaB_6 nanocrystalline with binding energies of Sr 3d at 132, 134 eV and Ba at 778, 794 eV, respectively. These experimental results of XPS have further characterized the surface information of CaB_6, SrB_6 and BaB_6 nanocrystalline.

The advantages of the present synthesis method are concluded as followings. (1) Although the maximum reaction temperature of present synthesis is 1150 ^oC holding for 2h, this temperature is relatively much lower than that of the synthesis for micron-size hexaborides powder indicating a characteristic of energy saving. Furthermore, the reaction process is easy controllable and the reaction does not require high pressure. (2) The average grain sizes of cubic shape CaB_6, SrB_6 and BaB_6 nanocrystalline are 150 nm, 20 nm and 30 nm at the reaction temperature of 1150 ^oC, which is the minimum value of literature reported so far. Meanwhile, this ultrafine grain size is more beneficial for exhibiting the plasmon resonance of nanoparticle. For the growth of cubic shaped alkaline-earth hexaborides in solid state system, its mechanisms have been proposed in Fig.7.

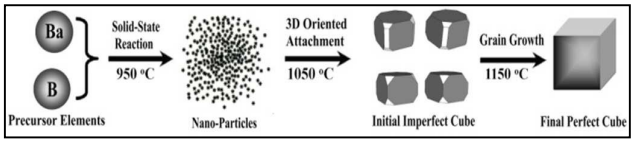

Fig.7 Schematic of the growth procedure of cubic shaped alkaline-earth hexaborides

3.3 Magnetic properties of MB_6 nanocrystalline

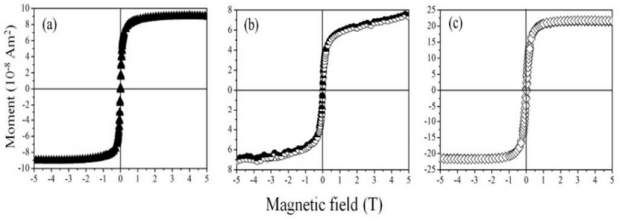

Fig.8 Room temperature magnetization curves for the MB_6 nanocrystalline prepared at 1150 ^oC (a) CaB_6 (b) SrB_6 (c) BaB_6

The room-temperature magnetization curve of the CaB_6, SrB_6 and BaB_6 nanocrystalline are obtained by subtracting off the diamagnetic background of the tetrafluoroethylene capsule. It can be seen from Fig.8 (a) that saturation magnetization of CaB_6 reach to M_s=9.0×10^{-8} A/m^2 indicating a weak ferromagnetic behaviors. Combining the measurement results of Fig.8 (b) and Fig.8 (c), we also see a weak ferromagnetic behaviors of SrB_6, BaB_6 and their saturation magnetizations are M_s=7.0×10^{-8} A/m^2 and M_s=22.0×10^{-8} A/m^2, which is our first time to report the ferromagnetic behaviors of the nanocrystalline alkaline-earth hexaborides. Although the available theoretical and experimental works predicting and explaining the ferromagnetism of MB_6 differ in details, many scientists more preferred to believe the intrinsic defects as a main factor leading to magnetic moments. In theory, the perfect structured MB_6 crystals show the zero local magnetic moment due to the high symmetry of spin up and down partial total density of states shown in Fig.9 (a) and Fig.9 (b), where we take the CaB_6 as an example to calculate. However, Cao *et al* [32] have theoretically found when the boron cage moves together in same direction shown in Fig.9 (c). This local lattice distortion contributed to large magnetic moments of CaB_6, which reason is explained that B atoms in CaB_6 crystal is negative charge and provide 1/3 extra electron producing the ferromagnetism. By experimentally, Lofland *et al* [28] have reported that the impurity phase of CaB_4O_7 not only increase the crystal defects but also enhance the local magnetic moments. Subsequently, Cho *et al* [33] synthesized the high quality and defect-controlled CaB_6 single crystal using the purity of 99.9999% and 99%

CrystEngComm Accepted Manuscript

 This journal is © The Royal Society of Chemistry 20xx

boron powder. As results, the single crystal prepared by the higher purity boron sources does not show ferromagnetic signal, which is well agreement with our calculation results of Fig.9 (a) and (b). But the crystal prepared by the 99% boron powder exhibited room temperature ferromagnetism. Based on the above mentioned works, it can be inferred that the magnetic moments of nanocrystalline MB_6 of present work is originated from the intrinsic defects rather than alien ferromagnetic elements. Because the EDS analysis of Fig.3 and Fig.5 have fully confirmed that there is no ferromagnetic element found in CaB_6, SrB_6 and BaB_6 nanocrystalline.

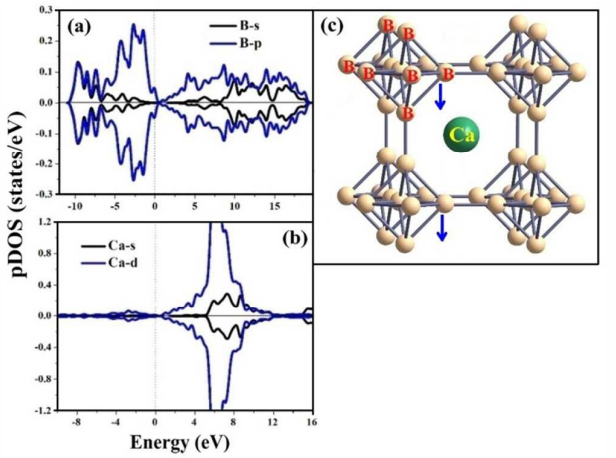

Fig.9 Projected density of states (PDOS) of CaB_6 (a) B atom, (b) Ca atom, (c) the sketch map of CaB_6 lattice distortion

However, up to now there is very rarely literature reported for the direct evidence of intrinsic defects for MB_6 (M=Ca, Sr and Ba) by experimentally. TEM as an effective characterization method is used to observe the crystal defects such as edge dislocation and lattice distortion. Fig.10 shows the HRTEM micrographs of crystal structure and inverse Fast Fourier Transformation patterns corresponding to CaB_6 and BaB_6 nanocrystalline. As seen in Fig.10 (a), the lattice fringes values of d=0.41 nm and d=0.24 nm agree well with the (100) and (110) crystal planes. Fig.10 (b) shows the inverse FFT patterns along the (100) crystal planes, where we clearly see the many edge dislocations and lattice distortions and those are indexed by yellow box. In same region, there also exist many edge dislocations in (110) crystal plane shown in Fig.10 (c). The detailed HRTEM analyses of BaB_6 crystal is shown in Fig.10 (d) and it is mainly composed of (100) and (111) crystal planes indexed in insert FFT pattern. Combining the inverse FFT of Fig.10 (e) with Fig.10 (f), the edge dislocations and lattices distortions are also observed from the selected single crystal. So, it is believed that the direct observation of edge dislocation and lattice distortion by HRTEM strongly supported the view that the magnetic moments of nanocrystalline alkaline-earth hexaborides are originated from the intrinsic defects. As for the formation of edge dislocation, it can be explained that the trace amounts of impurity element, mainly coming from the raw materials, is easy to form the vacancy and further hinder the crystallization during reaction procedure. This factor directly leads to the lattices dislocations effects.

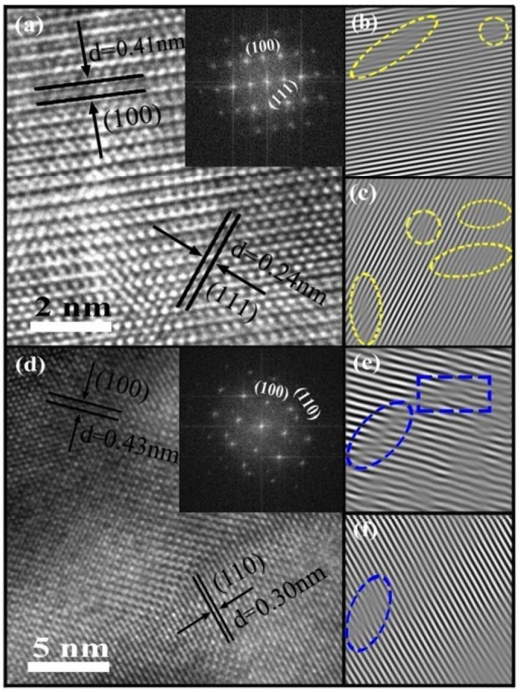

Fig.10 (a) HRTEM analysis of CaB_6, (b) and (c) inverse FFT patterns for (100) and (110), (d) HRTEM analysis of BaB_6, (e) and (f) inverse FFT patterns for (100) and (111)

3.4 Optical absorption properties of MB_6 nanocrystalline

CrystEngComm Accepted Manuscript

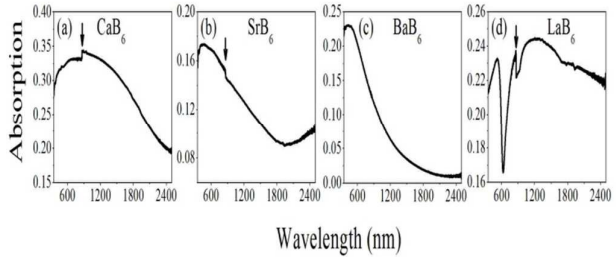

Fig.11 Absorption spectrum of MB_6 nanocrystalline from 350 nm to 2500 nm

Fig. 11 shows the absorption spectrum for MB_6 (M=Ca, Sr and Ba) nanocrystalline measured by the ultraviolet-visible-near infrared spectrometer. The interference peak at 860 nm marked by arrow is owing to the switching light source in the moment of measurement. It is notable from the absorption curve of CaB_6 nanocrystalline that there existed an strong wide absorption peak from ultraviolet region of 350 nm to near-infrared region of about 1800 nm and its intensity decreased with increasing the wavelength. By comparison with absorption curve of nanocrystalline SrB_6 (see in Fig.11b), the width of absorption peak became narrow and its peak position located at 467 nm, indicating a strong absorption capability of visible light. It is well known that at the position of absorption valley always accompany with minimum reflectivity and maximum transmission light. So it can be inferred from the absorption valley of SrB_6 that there exist an infrared light transmission for wavelength of 1935 nm. Meanwhile, it is interestingly found from the absorption curve of BaB_6 that the absorption peak moves toward lower wavelength of 421 nm and absorption valley is seems to become more smoothly. Combining the absorption property from Fig.11 (a) to Fig.11(c), we have found the nanocrystalline alkaline-earth hexaborides show a strong light absorption in visible light and transparency in near infrared rays. This optical absorption characteristic is much different from the nanocrystalline lanthanum hexaborides shown in Fig.11 (d), which date is taken from reference [34]. From the view point of practical application, the new absorption characteristic of nanocrystalline MB_6 should have important effects for extending the optical applications such as near infrared filtering or detectors.

4. Conclusions

In summary, the ultrafine alkaline-earth hexaborides MB_6 (M=Ca, Sr and Ba) nanocrystalline have been successfully synthesized by a novel method of single step, low cost and grain size controllable. The grain size and morphology of synthesized samples are very sensitive to the reaction temperature. The magnetic measurements results show that all the synthesized samples show a weak ferromagnetic behavior at room temperature, which is our first time to found the ferromagnetic property from nanocrystalline alkaline-earth hexaborides. Furthermore, the HRTEM observations strongly supported the evidence of intrinsic defect attributing to the magnetism. The optical absorption results show the nanocrystalline alkaline-earth hexaborides exhibited a strong light absorption in visible light and transparency in near infrared rays. This interesting optical property should have important effects for extending the optical applications such as near infrared filtering or detectors.

Acknowledgements

This work is supported by Fundamental Research Open Project of Inner Mongolia (Grant No. 20130902), National Natural Science Foundation of China (No. 51302129), Program for Young Talents of Science and Technology in Universities of Inner Mongolia (Grant No. NJYT-14-B03) and the High Level Talents Scientific Foundation of Inner Mongolia Normal University (Grant No. 2013YJRC017).

Notes and references

1 S. L Shang, Z. K. Liu, *Appl.Phys.Lett*., 2007, **90**, 091914.

2 G. E.Grechnev, A. E. Baranovskiy, V. D. Fil, T. V. Ignatova, I. G. Kolobov, A. V. Logosha, N. Shitsevalova, V. B. Filippov and O. Eriksson, *Low. Temp*., *Phys* 2008, **34**, 921.

3 K. M. Schmidt, A. B. Buettner, O. A. Graeveb, V. R. Vasquez, *J. Mater. Chem. C*., 2015, **3**, 8649.

4 X. Huang, J. C. Zhong, L.S. Dou, K. Wang, Int. *J. Refractory Metals & Hard Materials*., 2010, **28**, 143.

5 L.Zhang, G. H. Min, H. S. Yu, *Ceram. Int*., 2009, **l35**, 3533.

6 A. D. Liu, X. H. Zhang, Y. J. Qiao, *Ceram. Int*., 2014, **40**, 15997.

CrystEngComm Accepted Manuscript

 This journal is © The Royal Society of Chemistry 20xx

Please do not adjust margins

7 T. T. Xu, J. G. Zheng, A. W. Nicholls, S. S. Stankovich, R. D. Piner, R. S. Ruoff, *Nano Lett*., 2004, **4**, 2051.
8 P. Jash, A. W. Nicholls, R. S. Ruoff, M. Trenary, *Nano Lett*. 2008, **8**, 3794.
9 S. L. Zhou, J. X. Zhang, L. H. Bao, G. X. Yu, Q. L. Hu, D. Q. Hu, *J. Alloys Compd* 2014, **611**, 130.
10 M. Takeda, M. Terui, N. Takahashi, N. Ueda, *J. Solid State Chem* 2006, **179**, 2823.
11 M.Takeda, T. Fukuda, F. Domingo, T. Miura, *J. Solid State Chem*., 2004, **177**, 471-475.
12 M. Gursoy, M. Takeda, B. Albert, *J. Solid State Chem*., 2015, **221**, 191.
13 D. P. Young, D. Hall, M. E. Torelli, Z. Fisk, J. L. Sarrao, J. D. Thompson, H. R. Ott, S. B. Oseroff,; R. G. Goodrichk and R. Zysler, *Nature*., 1999, **397**, 412.
14 P.Vonlanthen, E. Felder, L. Degiorgi, H. R. Ott, *Phys. Rev. B*., 2000, **62**, 10076.
15 S. E. Lofland, B. Seaman, K. V. Ramanujachary, *Phys. Rev. B.,* 2003, **67**, 020410.
16 L. S. Dorneles, M. Venkatesan, M. Moliner, J. G. Lunney,; J. M. D. Coey, *Appl.Phys.Lett*., 2004, **85**, 6377.
17 K. Ackland, M. Venkatesan,; J. M. D. Coey, *J. Appl. Phys*., 2012, **111**, 07A322.
18 G. Q. Zhao, L. Zhang, L. J. Hu, H. Yu, G. H. Min,; H. S. Yu, *J. Alloys Compd* ., 2014, **599**, 175.
19 K. Matsubayashi, M. Maki, T. Tsuzuki, T. Nishioka, N. K. Sato, *Nature* 2002, **420**, 143.
20 M. H. Cao, J. Jiang, H. X. Liu, J. Yuan. *Physica B* 2005, **369**, 39.
21 T. Mori , S. Otani *Solid State Commun*., 2002, **123**, 287.
22 H. Zhang, Q. Zhang, G. P. Zhao, J. Tang, O. Zhou, L. C. Qin, *Adv. Mater*., 2006, **18**, 87.
23 S. L. Zhou, J. X. Zhang, D. M. Liu, Z. L. Lin, Q. Z. Huang, L. H. Bao, R. G. Ma, Y. F. Wei, *Acta Mater*., 2010, **58**, 4978.
24 R. Kanakala, R. Escudero, G. R. George, M. Ramisetty, O. A. Geaeve, *ACS Appl. Mat. Interfaces*., 2011, **3**, 1093.
25 R. Kanakala, G. R.George, O. A. Geaeve, *J. Am. Ceram. Soc*., 2010, **93**, 3136.
26 L. H. Xiao, Y. C. Su, X. Z. Zhou, H. Y. Chen, J. Tan. T. Hu, J. Yan, P. Peng, *Appl. Phys. Lett*., 2012, **101**, 041913.
27 Y. Sato, M. Terauchi, M. Mukai, T. Kaneyama, K. Adachi, *Ultramicroscopy*., 2011, **111**, 1381.
28 S. Schelm, G. B. Smith, *Appl. Phys. Lett*., 2003, **82**, 4346.
29 L. H. Bao, R. T. Y. Wu, W. Wei, O. Tegus, *Mater Charact.,* 2014, **97**, 69.
30 J. H. Ma, J. Li, G. X. Li, Y.G. Tian, J. Zhang, J. F. Wu, J. Y. Zheng, H. M. Zhuang, T. H. Pan, *Mater. Res. Bull*., 2007, **42**, 982.
31 S. Angappan, M. Helan, A. Visuvasam, L. J. Berchmans, V. Ananth, *Ionics*., 2011, **17**, 527.
32 J. X. Cao, Y. Zhu, Z. Q. Yang, R. Q. Wu, *Phys. Rev. B*., 2009, **79**, 132404.
33 B. K. Cho, J. S. Rhyee, B. H. Oh, M. H. Jung, H. C. Kim, Y. K. Yoon, J. H. Kim; T. Ekino, *Phys. Rev. B*., 2004, **69**, 113202.
34 L. M. Chao, L. H. Bao, J. J. Shi, W. Wei, O. Tegus, Z. D. Zhang, *J. Alloys Compd*., 2015, **622**, 618.

CrystEngComm Accepted Manuscript